Early-stage relaxation of hot electrons by LO phonon emission

Hervé Castella
Max-Planck-Institute für Physik Komplexer Systeme, Nöthnitzer Strasse 38, D-01187 Dresden, Germany

John W. Wilkins
Department of Physics, Ohio State University, 174 West 18th Avenue, Columbus, Ohio 43210-1106
(Received 27 September 1999)

Ultrafast spectroscopy gives insight into the relaxation and dephasing of electrons during the first femtoseconds after an optical excitation. A theoretical description of this early-time regime requires a proper treatment of retardation effects for the different scattering processes. The scattering of electrons by optical phonons is investigated within the *S*-matrix formalism. This perturbative scheme, equivalent to the non-equilibrium Green's function technique of Kadanoff and Baym [*Quantum Statistical Mechanics* (Benjamin, New York, 1962)], reproduces the phonon oscillations observed in four-wave mixing experiments on GaAs. The differential transmission spectrum, however, shows a sharper phonon replica than in experiments where additional dephasing mechanisms such as electron correlation effects may further broaden the replica.

I. INTRODUCTION

Ultrafast spectroscopy has brought much insight into the scattering of charge carriers during the first femtoseconds after an optical excitation.[1] In this early-time regime, both the coherence of the scattering processes and the energy uncertainty play essential roles.

The coherence induced by the laser is not completely lost during the first scattering processes, and quantum interference effects may lead to beatings in the optical response of the system. In particular oscillations with the LO-phonon frequency have been observed in four-wave mixing (FWM) experiments on GaAs, which were interpreted as evidence of memory effects.[2]

Non-energy-conserving processes play a significant role for times shorter than typical transition energies. In particular a sharpening of phonon satellites has been observed in differential transmission (DT) experiments, and interpreted as a signature of energy uncertainty in the early-time relaxation.[3]

The theory usually describes the excitation of charge carriers by the laser within semiconductor Bloch equations (SBE's), which give the time evolution of the density distributions in both bands, and of the interband polarization.[4] The scattering processes, however, are taken into account by instantaneous scattering rates as in Boltzmann equations, thus treating relaxation as totally incoherent and energy conserving.[5]

One of the most successful theoretical approach going beyond semiclassics is quantum kinetics, which describes the coupling to the light field as in SBE's, while the scattering terms depend on the system's past history.[6,7] These memory or so-called non-Markovian terms are deduced from non-equilibrium perturbation theory[8] by expressing two-time Green's functions with one-time density matrices, a procedure strictly valid only for noninteracting particles.[9] Despite this uncontrolled approximation, the quantum kinetics equations have successfully reproduced many of the experimental features of the coherent regime, such as phonon oscillations,[2] broad phonon satellites,[10] or the buildup of screening by excited carriers.[11]

Another approach to ultrafast dynamics describes the scattering processes via a hierarchy of equations for many-particle correlation functions, which is truncated to a closed set of equations by mean-field arguments. These methods encompass both the density-matrix approach which performs an expansion in coupling strength,[12–14] and the expansion in powers of the light field by Victor *et al.*[15] They have been extensively applied to relaxation by phonon emission[13,16,17] and Coulomb correlation effects.[18]

Purely quantum approaches, which avoid any of the above approximations necessary to have a closed set of equations, are usually not able to simulate nonlinear experiments on realistic models. Nonequilibrium Green's-function theory, which has been applied to both coupling to phonons[19] and to Coulomb correlations,[20] requires a large computational effort due to the explicit dependence of Green's functions on two-time variables. Several variational methods have also given insight into the memory effects for simplified low-dimensional models.[21,22] Recently, however, nonequilibrium Green's-function equations have been solved numerically with no further approximation for a realistic model of a semiconductor excited by a single pulse.[23]

The present work expands the *S*-matrix formalism introduced in Ref. 24 for electron interactions, to the coupling of electrons with phonons. This perturbative method is a purely quantum approach equivalent to the Green's-function theory, as shown explicitly here. However, it allows one to design approximations very similar to the variational methods, e.g., to restrict the scattering processes to states with few phonons. In contrast to the variational methods, the scheme is applied to realistic models for a bulk semiconductor and to nonlinear optical probes such as FWM or DT. An efficient algorithm is presented which solves Dyson's equation while avoiding any storage of two-time quantities.

In Sec. II, the model and the main results are described. Section III presents the formalism and the one-phonon approximation. Section IV illustrates the effect of energy un-

certainty on the phonon replica for a solvable one-dimensional model. The simulations of the DT experiments on GaAs are presented in Sec. V. The phonon oscillation in FWM is first studied for a solvable two-level system in Sec. VI, and for bulk GaAs in Sec. VII.

II. MODEL AND RESULTS

A two-band model describes a bulk semiconductor with a direct gap E_G and with band dispersions $\epsilon_{ck}=\hbar^2k^2/2m_c+E_G$ and $\epsilon_{vk}=-\hbar^2k^2/2m_v$ for the conduction and valence bands, respectively. The electrons interact via the Coulomb interaction $U(q)=e^2/\epsilon_0 q^2$. An external electromagnetic field $E(t)$ excites electrons from one band to the other with a dipole matrix element μ which is assumed to be independent of wave vector. Finally the electrons interact with an optical-phonon mode of flat dispersion at the frequency Ω via a Frölich coupling[25] $M_q^2=\hbar\Omega e^2(1/\epsilon_\infty-1/\epsilon_0)/2q^2$:

$$\hat{H}=\hat{H}_{el}+\hat{H}_{ph}+\hat{H}_{int},$$

$$\hat{H}_{el}=\sum_{\alpha k}\epsilon_{\alpha k}a^\dagger_{\alpha k}a_{\alpha k}-\left(\mu E(t)\sum_k a^\dagger_{vk}a_{ck}+\text{H.c.}\right)+\frac{1}{V}\sum_{\alpha\beta kk'q}U(q)a^\dagger_{\alpha k+q}a_{\beta k'}a^\dagger_{\beta k'-q}a_{\alpha k},\tag{1}$$

$$\hat{H}_{ph}=\hbar\Omega\sum_q b^\dagger_q b_q,$$

$$\hat{H}_{int}=\frac{1}{V^{1/2}}\sum_{k,q}M_q(a^\dagger_{ck+q}a_{ck}-a_{vk+q}a^\dagger_{vk})(b^\dagger_{-q}+b_q).$$

We focus here on optical excitations by short laser pulses, where electrons initially in the filled valence band are promoted into the conduction band and emit phonons. We want to describe the optical properties of the semiconductors in the first femtoseconds after the pulse when only a few phonons are created, and the electrons have not totally lost the phase coherence they acquired during the optical excitation.

A description of this early-time regime requires a proper treatment of retardation effects for the different scattering processes. We use the *S*-matrix formalism, which performs a perturbative expansion of creation and annihilation operators in different scattering channels.[24] This expansion is discussed in detail in Sec. III. The remaining part of the present section gives a brief account of the approximation used in our calculations and summarizes the main results.

The approximation restricts the scattering processes to those channels with at most one phonon in the final state, and treats the Coulomb interaction at the Hartree-Fock level. The coupling to the light $E(t)$, however, is computed exactly in order to have access to the nonlinear regime. The electron annihilation operators $a_{\alpha k}(t)$ have both a single-particle contribution $\tilde{g}_{\alpha\beta k}(t,0)a_{\beta k}$ and a phonon contribution which involves products of electron and phonon operators such as $a_{\beta k+q}(b_q+b^\dagger_{-q})$. The retarded Green's function $\tilde{g}$ satisfies Dyson's equation, with a self-energy accounting for emission and reabsorption of one virtual phonon: the so-called Born approximation. We now summarize the main results of this work.

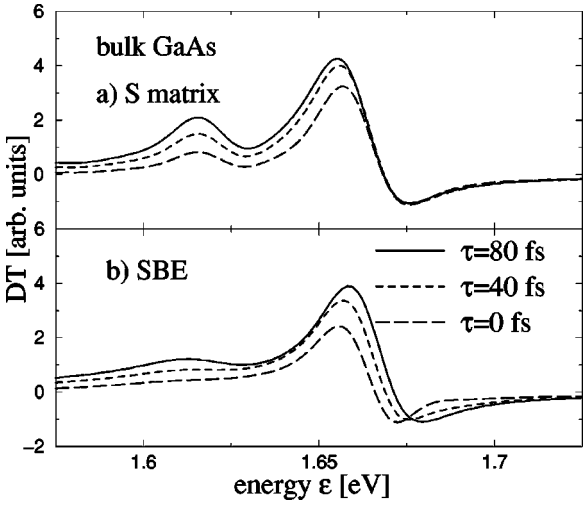

FIG. 1. Differential transmission (DT) signal computed with (a) the *S*-matrix formalism and (b) the semiconductor Bloch equations (SBE's) using as input the *S*-matrix results for the density distribution and for the interband polarization created by the pump pulse. The *S*-matrix results show a sharp phonon replica at lower energy even for zero time delay $\tau=0$, while the replica is very broad with the SBE's.

(1) We show in Sec. III that the *S*-matrix formalism is equivalent to nonequilibrium perturbation theory. However, it allows one to design variational-like approximations including a maximal number of phonons.

(2) An efficient algorithm is developed which does not require the storage of two-time quantities, and thus avoids much of the numerical problems encountered in Green's-functions calculations.[19,20] This procedure allows the simulation of nonlinear optical probes in a realistic model of a semiconductor within a fully quantum approach.

(3) The *S*-matrix formalism correctly reproduces the broad phonon replica in the density distribution of an electron relaxing by emission of phonons, as checked for both a solvable one-dimensional model in Sec. IV and for an optically excited semiconductor in Sec. V. The width of the replica is attributed to energy uncertainty which allows non-energy-conserving transitions for times smaller than the phonon period.

(4) The phonon replica in the DT signal shown in Fig. 1(a), is significantly sharper than in experiments on GaAs.[3] This result suggests that energy uncertainty alone cannot account for the broad replica observed experimentally, and that additional dephasing mechanisms such as electron correlation effects have to be included to reproduce the experimental findings.

(5) The sharp replica in DT contrasts with the broad features seen in the density distribution. In analogy to Ref. 16, this difference is attributed to interferences between phonon-scattering effects and optical excitation processes as discussed in Sec. V.

(6) The quantum beats in FWM are studied in Sec. VI for a two-level system where the *S*-matrix results compare very well with the exact $\chi^{(3)}$ response except for a renormalization of the beating frequency.

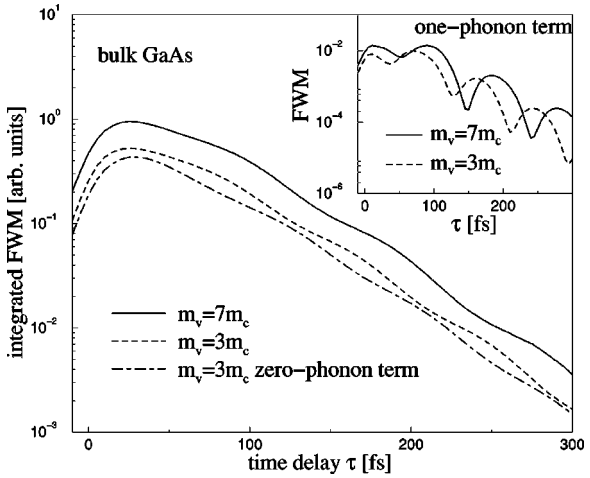

FIG. 2. Integrated four-wave mixing (FWM) signal as a function of time delay τ for a pump pulse of 15-fs duration centered at the exciton resonance of bulk GaAs. The oscillations due to phonon memory effects are particularly visible in the one-phonon contribution plotted in the inset. The period of the modulation is shorter than the bare phonon period $T_{ph}=115$ fs, and depends on the mass ratio m_v/m_c, as illustrated by changing the GaAs value of 7 to 3.

(7) The FWM is simulated in Sec. VII for the two-band model of GaAs. The *S*-matrix formalism quantitatively reproduces the phonon oscillations observed in experiments.[2] Figure 2 illustrates the dependence of the beating period on the mass ratio m_v/m_c, which is particularly clear in the one-phonon contribution to the signal, as shown in the inset.

III. FORMALISM

The *S*-matrix formalism perturbatively computes the time evolution of creation and annihilation operators in the Heisenberg picture. The diagrammatic technique was developed in Ref. 24, and applied to excitonic effects at the Hartree-Fock level. Here we implement the scheme for the electron-phonon model of Eq. (1) beyond the mean-field approximation to account for emission or absorption of a single phonon. We also outline the equivalence with the nonequilibrium perturbation theory,[8] and use the notation of Green's functions[26] instead of the original *S*-matrix language.

The section presents the general procedure for the *S*-matrix expansion, and then works out the mean-field approximation for the Coulomb interaction between electrons, and the non-self-consistent Born approximation for the coupling to phonons. Section III D gives the equations for the density matrix, and Sec. III E a brief account of the numerical algorithm.

A. General expansion

The electron annihilation operator at time t is formally expanded in scattering channels $a_{\alpha\ k}(t)=\Sigma_n a^{(n)}_{\alpha\ k}(t)$, where the channels involve an increasing number of phonons or particle-hole excitations with increasing order n. The different channels are orthogonal, $\langle\{a^{(n)}_{\alpha\ k}(t),a^{(m)\ \dagger}_{\alpha\ k}(t)\}\rangle=0$ for $n\neq m$, with the average computed in the initial state, i.e., a filled valence band and an empty conduction band without any phonon. The orthogonality is achieved via the normal ordering of electron and phonon operators, as explained in Appendix A.

The zeroth-order term $a^{(0)}_{\alpha\ k}$ describes the scattering of one electron initially in band α into band β without changing the number of phonons. It involves a single-electron operator and its amplitude is the retarded electron Green's function[27] $\tilde{g}_{\alpha\beta\ k}(t,0)$:

$$a^{(0)}_{\alpha k}(t)=\langle\{a_{\alpha k}(t),a^{\dagger}_{\beta k}(0)\}\rangle a_{\beta k}=i\tilde{g}_{\alpha\beta\ k}(t,0)a_{\beta k}. \quad (2)$$

The first order $a^{(1)}$ accounts for the emission or absorption of one phonon. It involves both an electron and a phonon operator, and its amplitude is a three-point correlation function with mixed electron and phonon characters:

$$a^{(1)}_{\alpha k}(t)=\frac{1}{V^{1/2}}\sum_q \langle\{a_{\alpha k}(t),a^{\dagger}_{\beta k+q}(0)b^{\dagger}_{-q}(0)\}\rangle a_{\beta k+q}b_{-q} + \langle\{a_{\alpha k}(t),a^{\dagger}_{\beta k+q}(0)b_q(0)\}\rangle a_{\beta k+q}b^{\dagger}_q. \quad (3)$$

Higher-order terms involve more complicated processes such as the emission of two phonons or the creation of a particle-hole pair. Appendix A describes the general procedure to construct orthogonal scattering channels $a^{(n)}$, and derives Eqs. (2) and (3). The rest of the paper, however, is restricted to the first two terms in the expansion.

The previous equations establish the connection between nonequilibrium Green's functions and the *S*-matrix formalism in contradiction to the claim of Ref. 24 that no such relation exists. In particular the usual diagrammatic technique for Green's function may be used to evaluate the *S*-matrix amplitudes as well. The *S*-matrix formalism, however, gives a clear picture of the many-body states involved for a given approximation.

B. Mean-field approximation

We first consider the mean-field equations for the Coulomb interaction without any coupling to phonons, as derived in Ref. 24. The retarded Green's function is a 2×2 matrix in the band indices with nonzero off-diagonal elements, since both the electric field and the Coulomb interaction couple the two bands. It satisfies a Schrödinger equation $i\partial_t g_k(t,t')=H^{(0)}_k(t)g_k(t,t')$, with the following Hamiltonian matrix:

$$H^{(0)}_k(t)=\begin{pmatrix}\epsilon_{ck} & -\mu E(t)\\ -\mu E^*(t) & \epsilon_{vk}\end{pmatrix}-\frac{1}{V}\times\sum_q U_q[g^{<}_{k+q}(t,t)-\rho]. \quad (4)$$

The Green's functions depend explicitly on both times t and t' due to the external light field which drives the system out of equilibrium. The Hartree-Fock term involving so-called lesser Green's function[26] $g^{<}_{\alpha\beta k}(t,t')=\langle a^{\dagger}_{\alpha k}(t)a_{\beta k}(t')\rangle$, accounts for the dynamical energy renormalization and for the excitonic coupling to the interband polarization. The last term, depending on the initial density matrix $\rho_{\alpha\beta}=\delta_{\alpha v}\delta_{\beta v}$, compensates for the interaction among valence electrons which is already included in the band gap.

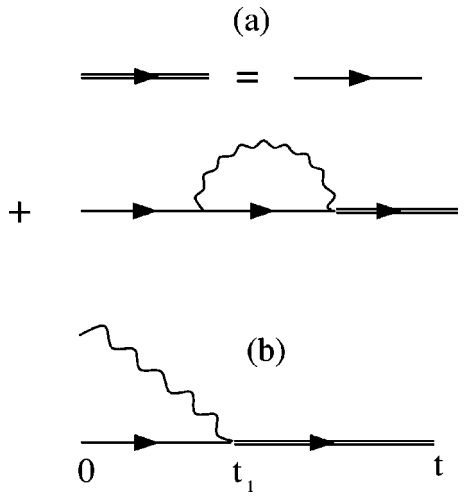

FIG. 3. Diagrams for the amplitude of (a) the zero-phonon term, i.e., the retarded Green's function, and of (b) the one-phonon term. Single straight lines are the unrenormalized electron Green's function in the presence of the light field and with excitonic effects at the Hartree-Fock level, and double lines the renormalized Green's function in the non-self-consistent Born approximation of (a). Wiggly lines denote the bare LO-phonon propagator.

C. Coupling to phonons

Our approximation restricts the scattering processes to the emission or absorption of at most one phonon, i.e., retains only $a^{(0)}$ and $a^{(1)}$ in the expansion. The consequent approximation for the renormalized retarded Green's function $\tilde{g}_k$ selects the diagrams describing the emission and reabsorption of one virtual phonon at a time, as depicted in Fig. 3(a). Within the self-energy σ_k the electron propagator is not renormalized since one virtual phonon is already present. Dyson's equations in this non-self-consistent Born approximation reads[19]

$$\tilde{g}_k(t,t') = g_k(t,t') + \int_{t'}^{t} dt_1 dt_2 \tilde{g}_k(t,t_1)\sigma_k(t_1,t_2)g_k(t_2,t'), \tag{5}$$

$$\sigma_k(t,t') = \frac{-i}{V}\sum_q M_q^2 \Theta(t-t')[g^{<}_{k+q}(t,t')e^{i\Omega(t-t')} + g^{>}_{k+q}(t,t')e^{-i\Omega(t-t')}]. \tag{6}$$

The amplitudes of $a^{(1)}$ in Eq. (3) are approximated similarly by selecting diagrams with at most one phonon line at a time as shown in Fig. 3(b). The electron Green's function is not renormalized for times smaller than t_1 since a real phonon is present, and no virtual phonon excitations are allowed. At later times, however, the real phonon has been absorbed, and virtual phonon excitations are taken care of within the renormalized $\tilde{g}_k$. The corresponding formula for $a^{(1)}$ reads

$$a^{(1)}_{\alpha k}(t) = i\int_0^t dt_1 \tilde{g}_{\alpha\beta\ k}(t,t_1)\frac{1}{V^{1/2}}\sum_q M_q(e^{i\Omega t_1}b^{\dagger}_q + e^{-i\Omega t_1}b_{-q})g_{\beta\gamma\ k+q}(t_1,0)a_{\gamma\ k+q}. \tag{7}$$

The subtle mixture of renormalized and bare Green's function in the above equation, that we have motivated in physical terms, is necessary to provide consistent approximations for both $a^{(1)}$ and the self-energy. In particular it ensures that the Green's function obtained by inserting the operator $a_{\alpha k} = a^{(0)}_{\alpha k} + a^{(1)}_{\alpha k}$ into the definition of the retarded Green's function $\tilde{g}_k(t,t') = -i\langle\{a_{\alpha k}(t), a^{\dagger}_{\beta k}(t')\}\rangle\Theta(t-t')$ does satisfy Dyson's equation. This procedure corresponds graphically to combining two diagrams of Fig. 3(b) into the self-energy contribution of Fig. 3(a).

D. Density matrix

Finally, we need to compute the observables at time t, i.e., the renormalized lesser Green's function $\tilde{g}^{<}_k(t,t)$ or the density matrix. The orthogonal channels give separate contributions to the density matrix:

$$\tilde{g}^{<}_{\alpha\beta k}(t,t) = \langle a^{(0)\dagger}_{\beta k}(t)a^{(0)}_{\alpha k}(t)\rangle + \langle a^{(1)\dagger}_{\beta k}(t)a^{(1)}_{\alpha k}(t)\rangle, \tag{8}$$

$$\langle a^{(0)\dagger}_{\beta k}(t)a^{(0)}_{\alpha k}(t)\rangle = (\tilde{g}_k(t,0)\rho\tilde{g}^{\dagger}_k(t,0))_{\alpha\beta}, \tag{9}$$

$$\langle a^{(1)\dagger}_{\beta k}(t)a^{(1)}_{\alpha k}(t)\rangle = \frac{1}{V}\sum_q M_q^2 \int_0^t \times dt_1 dt_2 e^{i\Omega(t_1-t_2)}[\tilde{g}_k(t,t_1)g_{k+q}(t_1,0) \times \rho g^{\dagger}_{k+q}(t_2,0)\tilde{g}^{\dagger}_k(t,t_2)]_{\alpha\beta}. \tag{10}$$

The density distribution in each band $\tilde{g}^{<}_{\alpha\alpha k}$ is strictly positive, since the contribution of channel n is the norm of the vector $a^{(n)}_{\alpha k}(t)|\psi(0)\rangle$, with $|\psi(0)\rangle$ denoting the initial state. This positivity is in sharp contrast with the situation encountered in quantum kinetics or density-matrix formalism, where the distributions may become negative.[6,13]

The total number of particles is not conserved in the one-phonon approximation, since it is not self-consistent. In our calculations, however, the number of conduction electrons and valence holes never differed more than by a few percent.

E. Numerical implementation

Here we show how to avoid working explicitly with two-time Green's functions in the numerical solution of Dyson's equations, and then we describe the main aspects of the numerical algorithm. The details are presented in Appendix B.

The evaluation of Eq. (10) requires Green's functions for both final and intermediate times t and t', respectively. Working with a two-time Green's function posed storage problems in Ref. 19 which were resolved by drastically limiting the so-called memory depth $t-t'$, as well as the number of discretization points in momentum space. Here we show how to avoid any such problem within our non-self-consistent Born approximation.

Within the mean-field approximation, the lesser and greater Green's functions are related to a product of retarded Green's functions with one time argument fixed at the initial time:

$$g^{<}_k(t,t') = g_k(t,0)\rho g^{\dagger}_k(t',0),$$

$$g_k^>(t,t') = g_k(t,0)(1-\rho)g_k^\dagger(t',0). \tag{11}$$

These relations have two important implications: (1) We avoid storing the two-time Green's function, and need retarded functions with the second argument fixed at the initial time. The reduction of memory usage is important for simulations of short-pulse excitations which require a large energy cutoff and small time increments. (2) The self-energy in Eq. (6) factorizes into products of terms depending either on t or on t'. As shown explicitly in the Appendixes, this factorization allows us to break the second-order differential equation into a set of first-order equations, in close analogy to the procedure used in quantum kinetics.[6]

The numerical solution of the *S*-matrix equations has the following steps: (a) The mean-field equations (4) are solved using a time increment sufficiently small to resolve the short laser pulses; (b) the retarded Green's functions $\tilde{g}_k(t,0)$ for a given momentum k and final time t are computed by solving Dyson's equation; and (c) the one-phonon contribution in Eq. (10) can be simultaneously evaluated, as shown in Appendix B.

The stability of the numerical integration of Dysons's equation allows us to work with a large time increment $\Omega dt \simeq 0.1$ without significant loss of precision. The number of k points is reduced by using the rotational symmetry of the Green's function.[6] In practical calculations we used a discretization of energy $\hbar^2k^2/2m_e$ rather than momentum.

IV. SINGLE ELECTRON IN ONE DIMENSION

Here we illustrate the importance of the energy uncertainty within the simplified problem of a single electron relaxing by emission of optical phonons. In the early-time regime the phonon satellites in the energy distribution function are very broad, and sharpen after typically one phonon period. Furthermore we compare the exact electron distribution function to Boltzmann kinetics and to the *S*-matrix predictions for a solvable one-dimensional model.[28] The benchmarking results show that the broad phonon replicas are not captured by semiclassics,[13,16,21] but are correctly reproduced in early times by the *S*-matrix formalism. The one-phonon approximation, however, breaks down for times larger than the electron lifetime when two-phonon processes become important.

The one-dimensional model describes a single electron in a conduction band with linear dispersion $\epsilon_{ck}=k$ and a single branch extending to $\pm\infty$. The coupling to phonons is independent of the momentum transfer $M_q=\eta$. The electron is initially prepared at an energy k_0 high in the band in order to mimic the nonequilibrium situation created by an optical excitation.

Within Boltzmann kinetics, the energy-distribution function consists of δ functions at energies $k_0-m\Omega$, $m=0,1,\ldots$, with weights $\exp(-\eta\tau)(\eta\tau)^m/(m!)$. The amplitude of the main peak at k_0 decays exponentially with a typical lifetime η^{-1}, while the mth phonon satellite grows within a time interval of $m\eta^{-1}$.

The exact distribution function computed in Ref. 28 is compared in Fig. 4 to Boltzmann kinetics for different times τ. The main peak at energy $k_0=3.5\Omega$ is exactly described by semiclassics. The first phonon satellite, however, which is a

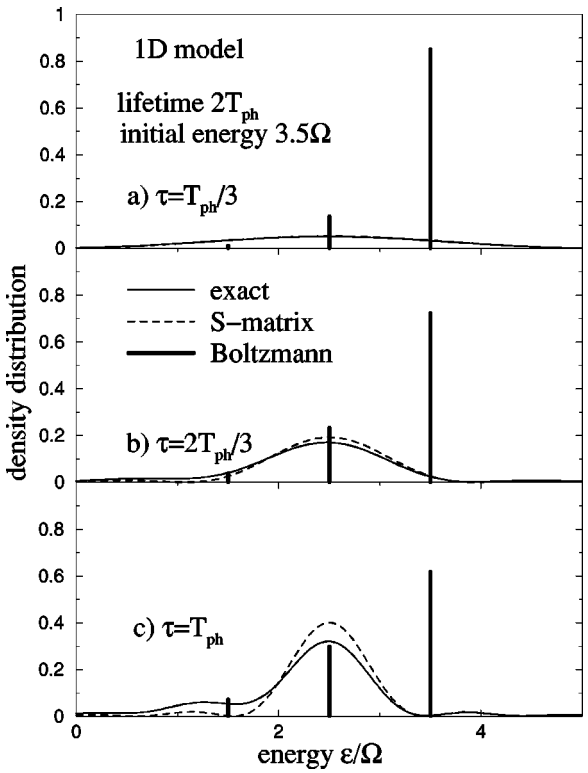

FIG. 4. Electron-density distribution as a function of energy ϵ for a single electron coupled to LO phonons in the exactly solvable one-dimensional model with linear band dispersion. The electron is prepared initially at $\tau=0$ with an energy $\epsilon=3.5\Omega$, and the electron lifetime is twice the phonon period. The phonon replica at $\epsilon \simeq 2.5\Omega$ is initially very broad within the exact solution, in contrast to the Boltzmann result which consists of δ functions building up as time increases. The broad phonon replica is well reproduced by the *S*-matrix formalism at early times, while discrepancies with the exact solution show up at $\tau=T_{ph}$ when the second phonon replica begins to develop.

δ function in Boltzmann's result, is initially very broad for the exact result, and only after one phonon cycle T_{ph} does a well-defined maximum appears at the energy $k_0-\Omega=2.5\Omega$. This discrepancy is caused by non-energy-conserving transitions which are not included in semiclassics, but play an essential role in the exact solution for times shorter than the phonon period.

Now we turn to the *S*-matrix formalism, where the time evolution of the distribution $\tilde{g}_k^<(\tau,\tau)$ is readily computed analytically. The decay of the peak at k_0 is exact, while the first phonon satellite has a Lorentzian shape centered at $k_0-\Omega$:

$$\tilde{g}_k^<(\tau,\tau) = e^{-\eta\tau}\left(\delta(k-k_0)+\eta^2\left|\frac{e^{\eta\tau/2+i(\Omega+k-k_0)\tau}-1}{\eta/2+i(\Omega+k-k_0)}\right|^2\right). \tag{12}$$

Figure 4 shows how the broad first phonon satellite is correctly reproduced by the S matrix for $\tau<T_{ph}$ in sharp contrast to Boltzmann kinetics. The *S*-matrix result, however, departs from the exact distribution when the second phonon replica starts to grow at times larger than the electron lifetime $\tau>\eta^{-1}=2T_{ph}$. This failure is clearly due to our approximation retaining only one-phonon processes.

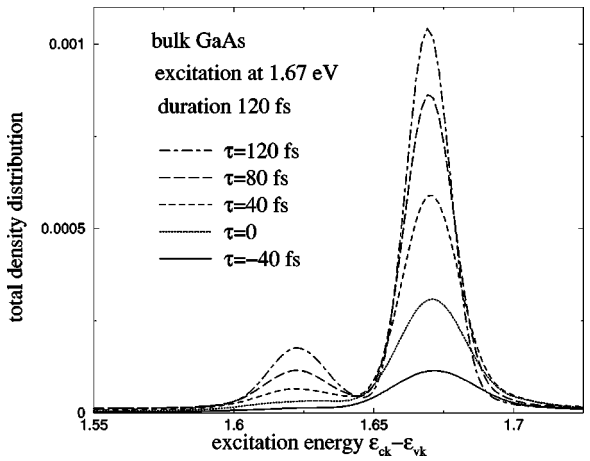

FIG. 5. Total density distribution as a function of excitation energy $\epsilon_{ck}-\epsilon_{vk}$ for bulk GaAs excited by a 120-fs pulse of 150-meV excess energy. The phonon satellite at 1.63 eV is initially very broad, and starts peaking at 80 fs after the pulse.

V. DIFFERENTIAL TRANSMISSION

This section studies the growth of phonon satellites for the two-band model of Eq. (1) for bulk GaAs. We compute both the density of carriers excited by the pump pulse and the full DT signal. The phonon replicas in the density distribution are broad at early times due to energy uncertainty while the DT signal shows sharper structures due to interferences between scattering with phonons and optical excitation.

Figure 5 shows the total density distribution of conduction electrons and valence holes as a function of interband excitation energy $\epsilon_{cv}-\epsilon_{vk}$ for different times after the pump pulse. The system is excited by a 120-fs pulse centered at 150 meV above the band gap as in Ref. 3's experiment. At early times the main peak at 1.67 eV shows a broad tail on the low-energy side. At 40 fs after the pulse a distinct maximum appears at 1.63 eV, where the phonon replica starts to grow. The energy separation between the main peak and the satellite is $(1+m_c/m_v)\hbar\Omega=40$ meV, which is larger than the phonon frequency $\hbar\Omega=36$ meV due to the band dispersion.[3] The width of the replica changes from approximately 40 meV at $\tau=40$ fs to 25 meV at $\tau=120$ fs, which is significantly larger than the main peak width of 20 meV.

The broad tail at early times and the sharpening of the replica can be attributed to the energy uncertainty as in the one-dimensional (1D) model of Sec. IV. Indeed for times smaller than the phonon period non-energy-conserving processes cause the broad features in Fig. 4(a), which are very similar to the present observations. Semiclassical calculations do not capture these memory effects in both two-band and 1D models since they predict the same width for both the phonon replica and the main peak.[10,16]

Our results compare very well with the density-matrix simulation of Ref. 16, where memory effects were included via electron-phonon correlation functions. The quantum kinetics calculations of Ref. 10, however, show broader replicas with a well-defined maximum only for delays larger than 100 fs. The discrepancy may be attributed to a tendency of quantum kinetics to overestimate the self-energy effects. Below we show that this difference is even more pronounced in the DT signal.

The DT response is the change in transmission of the probe pulse induced by the pump, and roughly measures the occupation of the conduction band by optically excited electrons. The transmission is computed numerically by using the well-known projection of the polarization onto the transmitted direction q_2, where q_2 and q_1 are the propagation directions of the probe pulse E_2 and the pump pulse E_1, respectively.[30] The spatial dependence of the slowly varying fields is replaced by a fixed phase difference ϕ, $E_1(t)=E(t)$ and $E_2(t)=e^{i\phi}E(t-\tau)$, with a Gaussian pulse shape $E(t)=E_0e^{i\omega_0 t}\exp(-(\Delta t)^2)$ in the rotating-wave approximation. The interband polarization is computed for different phases ϕ, and the DT signal is obtained by numerical projection onto the first harmonics $\exp(i\phi)$.

Figure 1(a) shows the DT signal computed with the *S*-matrix formalism for the same excitation conditions as in Fig. 5, and various time delays τ. The main peak at 1.66 eV is redshifted compared to the density distribution and a decrease in transmission occurs 1.68 eV due to exciton effects as seen in experiments[3] and in quantum-kinetic calculations.[10] However a maximum at 1.62 eV is observed even for zero time delay, and the phonon replica is much sharper than both in experiments and in the density distribution plotted in Fig. 5. Below we discuss first the difference between DT and density, and finally the discrepancy with experiments.

Here we show that the difference between DT and density does not come from a simple interference between the pump and probe pulse. We compute the DT response within the SBE equations of Ref. 31, using as input the *S*-matrix calculations of the density distribution and of the interband polarization due to the pump alone. This procedures differs from the one in Refs. 3 and 32, where the density distribution from the 1D model was used while the polarization effects were neglected. The DT signal from the SBE plotted in Fig. 1(b) shows a much broader phonon replica than in the *S*-matrix results. Therefore the sharp replica observed with the *S*-matrix approach cannot be attributed to a simple interference effect between pump and probe which would be captured by the SBE's.

The sharp replica must have its origin in more subtle interference effects which are absent from the SBE calculations. In particular we attribute the sharp phonon replica to interferences between phonon scattering and optical excitation by the probe, in analogy to the density-matrix calculations of Ref. 16, where such interference terms have produced a sharpening of the replica.

In conclusion we discuss the discrepancy between the computed DT signal and the experiments. Our calculations show that the phonon replica in DT are very sensitive to the coherence between phonon scattering and optical excitation. Additional dephasing mechanisms such as electron correlation effects would reduce this coherence, and further broaden the phonon replica. A full self-consistent treatment of Dyson's equation could also contribute to a further broadening, as seen in the quantum-kinetic calculations of Ref. 10.

VI. TWO-LEVEL SYSTEM

In this section, an exactly solvable two-level system gives us insight into the origin of the quantum beats observed in

FWM experiments[2] on GaAs, as well as benchmarking results for the *S* matrix in the weak-coupling regime. For both linear response to the field and the FWM signal, the main discrepancy between *S*-matrix and exact results is the renormalization of the beating frequency.

The two-level model describes an electron coupled to a single oscillator, and mimics in a crude way the valence and conduction bands of the semiconductor. An electric field $E(t)$ causes interlevel transitions:

$$\hat{H}_2=\sum_{i=0}^{1}\epsilon_i a_i^\dagger a_i+\Omega b^\dagger b+\eta a_1^\dagger a_1(b+b^\dagger)-E(t)a_0^\dagger a_1 - E^*(t)a_1^\dagger a_0. \tag{13}$$

The exact eigenstates for $E(t)=0$ are polaronic states, i.e., superpositions of states with different numbers of phonons.[33] The energy levels for a fixed electronic level are separated by exactly the phonon energy: $E_{0n}=\epsilon_0+n\Omega$ and $E_{1n}=\epsilon_1+n\Omega-\eta^2/\Omega$ for levels 0 and 1, respectively.

The interlevel polarization $\tilde{g}_{10}^{<}(t,t)$ in linear response to the field was computed exactly in Ref. 25 in connection to phonon broadening of impurity levels. It has oscillations at multiples of the phonon period, which are a signature of the polaronic nature of the eigenstates:

$$\tilde{g}_{10}^{<}(t,t)=i\Theta(t)\exp\left[-i\left(\epsilon_1-\frac{\eta^2}{\Omega}-\epsilon_0\right)\cdot t - \left(\frac{\eta}{\Omega}\right)^2\right]\sum_{m=0}^{\infty}\left(\frac{\eta}{\Omega}\right)^{2m}e^{-im\Omega t}. \tag{14}$$

We now compare the exact linear response to the *S*-matrix result. The 2×2 self-energy matrix σ_{ij} in the level indices has only a single nonvanishing term for $i=j=1$, since the oscillator couples to the upper level only. In close analogy to Eq. (6), it reads

$$\sigma_{11}(t,t')=-i\eta^2\Theta(t-t')[e^{i\Omega(t-t')}g_{11}^{<}(t,t') + e^{-i\Omega(t-t')}g_{11}^{>}(t,t')]. \tag{15}$$

In addition to this contribution, a Hartree-Fock (HF) term remains,[34] which is absent in the two-band model because of order $V^{-1/2}$ in the volume V:

$$\sigma_{11}^{HF}(t,t')=-2\eta^2\delta(t-t')\int_0^t \sin[\Omega(t-t_1)]g_{11}^{<}(t_1,t_1)dt_1. \tag{16}$$

Within the *S*-matrix formalism the polarization to linear order has only two oscillating contributions at frequencies $\omega_\pm=\Omega(1\pm x)/2$ with $x=\sqrt{1+4(\eta/\Omega)^2}$:

$$\tilde{g}_{10}^{<}(t,t)=i\Theta(t)e^{-i(\epsilon_1-\epsilon_0)t}[(1+x)e^{-i\omega_- t} + (x-1)e^{-i\omega_+ t}]/2x. \tag{17}$$

Comparing the exact polarization to the *S*-matrix result, we see that the lowest frequency ω_- is correctly reproduced to second order in η, while the excitation energy $\omega_+-\omega_-=x\Omega$ is too large by an amount $2\eta^2/\Omega$. As shown below this discrepancy is also present in the FWM result.

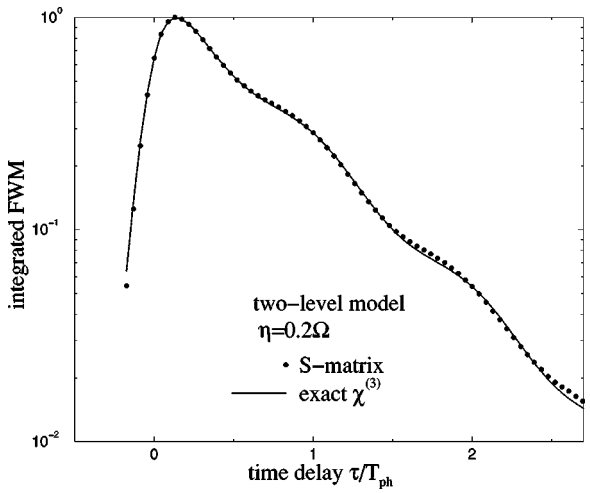

FIG. 6. Integrated FWM intensity as a function of time delay τ within the two-level model with a weak coupling ($\eta=0.2\Omega$) to a single-phonon mode. The *S*-matrix result is compared to the exact third-order response $\chi^{(3)}$ for a pulse duration of $0.12T_{ph}$ and a weak-field amplitude $\mu E_0=0.1\Omega$. The amplitude of the phonon oscillations in the exact result are very well reproduced by the *S* matrix, while their period is slightly smaller than the phonon period T_{ph} due to the erroneous renormalization of the excitation frequency.

The FWM response comes from the diffraction of the probe in direction $2q_2-q_1$ by the polarization created by a first pulse, where q_1 and q_2 are the propagation directions of the first and second pulses, respectively. It is computed numerically within the *S*-matrix formalism with the same projection technique presented in the previous section for the DT signal. Here the polarization is projected onto the second harmonics $\exp(2i\phi)$ to pick up the right diffracted direction.

Figure 6 shows the FWM intensity integrated over real time t as a function of time delay τ, with an additional phenomenological damping $\Gamma=0.8/T_{ph}$ to perform the time integration. It compares the *S*-matrix result to the exact third-order response[35] $\chi^{(3)}$ in the weak-coupling regime $\eta=0.2\Omega$. The *S*-matrix formalism reproduces the weak oscillations at positive time delay due to quantum beats between states with different number of phonons. As in linear response, the slight change in oscillation frequency is attributed to the wrong excitation frequency $\omega_+-\omega_-\simeq1.08\Omega$ instead of the bare phonon frequency.

From the benchmarking results on the two-level system, we can conclude that the *S*-matrix formalism does reproduce the quantum beats due to emission of virtual phonons, but introduces an erroneous renormalization of the oscillation frequency.

VII. FOUR-WAVE MIXING

This section presents the simulation of the FWM experiments on bulk GaAs using the two-band model and the projection technique outlined in Sec. V. The integrated FWM oscillates as a function of time delay with a period smaller than the bare phonon period due to band-dispersion effects. This renormalization of the period is not an artifact of per-

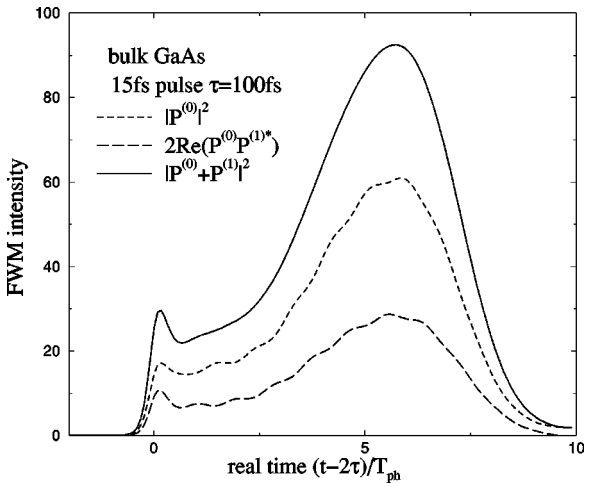

FIG. 7. FWM intensity as a function of real time for 15-fs pulses delayed by 100 fs and resonant with the excitonic level. The total signal is separated into a zero- and one-phonon contributions, $P^{(0)}$ and $P^{(1)}$, respectively. The total intensity $|P^{(0)}+P^{(1)}|^2$ is dominated by the undamped oscillations at the excitonic frequency but shows no modulation at the LO-phonon frequency Ω. The zero-phonon term $|P^{(0)}|^2$ shows weak oscillations at the frequency Ω, which are totally compensated for by the mixed term $P^{(0)}P^{(1)}*$.

turbation theory as in the two-level model. The FWM intensity in real time shows no modulation with the LO frequency, but is dominated by excitonic effects. Both features are consistent with experimental data and with quantum-kinetic results.[2]

Figure 7 shows the total FWM intensity as a function of real time for two pulses of 15-fs duration delayed by $\tau = 100$ fs, and resonant with the excitonic level. The signal starts at time $t=2\tau$ as a typical echo and shows a large maximum at $t=2\tau+5T_{ph}$ due to excitonic effects. The signal is dominated by the excitonic resonance which is indeed undamped at zero temperature, since the states close to the band edge cannot emit any real LO phonon.

While the total signal does not show any modulation with the phonon period, the zero- and one-phonon channels contribute oscillating terms $P^{(0)}(t,\tau)$ and $P^{(1)}(t,\tau)$, respectively. The modulation at frequency Ω, which is present in the zero-phonon contribution $|P^{(0)}|^2$, is suppressed by the mixed term $P^{(0)}P^{(1)}*$ oscillating out of phase. A similar cancellation occurs in the linear-response polarization due to vertex corrections.[36]

Figure 2 shows the integrated intensity $I(\tau)$ as a function of time delay τ:

$$I(\tau)=\int e^{-\Gamma t}|P^{(0)}(t,\tau)+P^{(1)}(t,\tau)|^2 dt. \qquad (18)$$

In contrast to the real-time behavior, the oscillations at approximately the phonon period are clearly present both in the total signal and in the one-phonon contribution.

The period of the oscillations depends on the mass ratio m_v/m_c between valence and conduction band, as shown clearly in the inset of Fig. 2. While the two-level model predicted oscillations at the bare phonon frequency, the period here changes from $T_{ph}=115$ fs to approximately 100 fs for a mass ratio $m_v/m_c=7$ as in GaAs, and to 85 fs for a ratio of 3.

The change in period was interpreted in Ref. 2 as an interference between two interband transitions whose energy differ by $\Omega(1+m_c/m_v)$. The first transition at momentum k has energy $\epsilon_{ck}-\epsilon_{vk}$, and the second one occurs at the momentum k', where the conduction electron decays after emitting one phonon: $\epsilon_{ck'}=\epsilon_{ck}-\Omega$. The energy difference $\epsilon_{ck'}-\epsilon_{vk'}-\epsilon_{ck}+\epsilon_{vk}$ gives the above-mentioned energy which correctly reproduces the frequency observed in the simulations. This argument, however, does not apply to excitations at the exciton level since an electron close to the band edge cannot emit any real phonon. It is more relevant to nonresonant excitations well above the band edge as in Sec. V.

This period change is not an artifact of perturbation theory, as in the two-level model. Following Ref. 29 the erroneous frequency renormalization, which is due to the polaron shift, can be estimated for an exciton in the $1S$ state to be $\Omega\alpha_F\sqrt{m_v/m_c}/16$, where α_F is the polaron constant. This very small shift of approximately 0.01Ω for GaAs parameters would also decrease with decreasing mass ratio m_v/m_c, in contrary to what is seen in Fig. 2.

The absence of oscillations in real time, points to differences with the simple quantum-beat picture drawn from the two-level system where the superposition of states with energy difference Ω causes oscillations in the FWM intensity: $|P^{(0)}+P^{(1)}|^2\propto g^2|2e^{i\Omega\tau}-e^{i\Omega t}-1|^2$. The absence of oscillations in the three-beam experiment of Ref. 37 is another indication of the difference between simple quantum beats as observed in quantum dots,[38] and the LO-phonon oscillation observed in bulk GaAs.

VIII. CONCLUSIONS

In this work we have developed the *S*-matrix formalism for a nonlinear optical probe of a bulk semiconductor with coupling to LO phonons. We have shown that the formalism is equivalent to nonequilibrium perturbation theory, but that it allows one to design simple physical approximations in the same spirit as variational methods. The one-phonon approximation has been implemented numerically with an efficient numerical algorithm which avoids the storage of two-time correlation functions as is typical in Green's function theory, and which allows us to simulate realistic experimental situations.

The relaxation of electrons by the emission of phonons has been studied for an ultrafast optical excitation. The phonon replica in the density distribution is initially very broad due to energy uncertainty, and sharpens after one phonon period. The DT signal, however, exhibits much sharper structures even at zero time delay. This difference between DT and density is explained in terms of interferences between phonon scattering effects and optical excitation.

The phonon replica in DT are also much sharper than experimentally observed. This suggests that additional dephasing mechanisms such as electron-electron scattering which would partially destroy the interference effect, are necessary to explain the experimental broad replicas.

The phonon oscillations observed in FWM experiments on GaAs are correctly reproduced by our simulations. The

period of the oscillations is consistent with the band dispersion effect proposed in Ref. 2. However, it is still unclear why such explanation involving excitations high in the band, should apply to an excitation at the band edge as in the experiments.

In conclusion, the *S*-matrix formalism provides a fully quantum approach to ultrafast dynamics in semiconductors which captures most of the memory effects. Since it is an expansion in number of phonons, it is restricted to the early-time regime, where only a few phonons are emitted.

ACKNOWLEDGMENTS

We thank A. V. Kuznetsov and R. Zimmermann for stimulating discussions. This work was supported by the Swiss National Science Foundation, by the U.S. DOE-Basic Energy Sciences, Division of Material Sciences and the Max-Planck Gesellschaft.

APPENDIX A: *S*-MATRIX FORMALISM

This appendix gives the general procedure to expand the electron operator $a_{\alpha k}$ in scattering channels and proves Eqs. (2) and (3) relating the *S*-matrix formalism to nonequilibrium Green's-function theory.[8]

A perturbative expansion of the annihilation operator $a_{\alpha k}$ in the electron-phonon coupling $\hat{H}_{int}$ generates commutators such as $[\ldots[a_{\alpha k},\hat{H}_{int}],\ldots,\hat{H}_{int}]$ which involve products of many annihilation or creation operators in various orders. A well-defined expansion requires a specification of the ordering of operators, and here we use the normal ordering with respect to the noninteracting initial state, i.e., a filled valence band and an empty conduction band with no phonon present. This choice provides an expansion $a_{\alpha k}=\Sigma_n a_{\alpha k}^{(n)}(t)$ in orthogonal contributions $\langle a_{\alpha k}^{(n)\dagger} a_{\alpha k}^{(m)}\rangle = 0$ for $n\neq m$, since the average of two normal-ordered operators $:A_1\ldots A_n:$ and $:B_1\ldots B_n:$ vanishes unless they are Hermitian conjugate to each other, up to a sign change.

The main outcome of the previous formal manipulations is the equivalence between the *S*-matrix formalism and nonequilibrium Green's functions. Indeed the amplitude of the first term $a_{\alpha k}^{(0)}=S_{\alpha\beta k}^{(0)}(t,t_0)a_{\alpha k}$ is proportional to the retarded Green's function $\tilde{g}_{\alpha k}$ due to the orthogonality between $a^{(0)}$ and higher-order terms:

$$\tilde{g}_{\alpha\beta k}(t,0) = -i\langle\{a_{\alpha k}(t),a_{\beta k}^{\dagger}\}\rangle = -i\langle\{a_{\gamma k}^{(0)}(t),a_{\beta k}^{\dagger}\}\rangle = -iS_{\alpha\beta k}^{(0)}(t,0). \quad \text{(A1)}$$

In a similar way the scattering channel $a^{(1)}$ involves products of operators $a_{\beta k-q}b_q$ which are orthogonal to $a_{\beta k}$ and any other higher-order channels, and whose amplitude is the three-point correlation function as given by Eq. (3):

$$\langle\{a_{\alpha k}(t),a_{\beta k-q}^{\dagger}b_q^{\dagger}\}\rangle = \langle\{a_{\alpha k}^{(1)}(t),a_{\beta k-q}^{\dagger}b_q^{\dagger}\}\rangle. \quad \text{(A2)}$$

APPENDIX B: NUMERICAL ALGORITHM

This appendix presents the algorithm to solve Dyson's equations and to compute the renormalized lesser Green's functions. The time evolution of the bare Green's function $g_k(t,0)$ is first computed straightforwardly by solving the mean-field equation for the 2×2 Hamiltonian matrix in Eq. (4). The renormalized retarded and lesser Green's functions for a given momentum k and final time t are obtained by solving a linear equation for a large vector $\vec{y}(t')$ whose first element is proportional to the retarded Green's function: $y_0(t')=\tilde{g}_k(t,t')g_k(t',0)$. The other components describe the amplitude of probability for the states with one phonon and the electron with momentum k_m, where the momenta have been assigned a particular ordering labeled by $m=1,N$, N being the maximal number of k points:

$$y_m(t') = i\int_{t'}^{t} y_0(t_1)h_m(t_1), \quad \text{(B1)}$$

$$h_m(t') = [\rho e^{-i\Omega t'} + (1-\rho)e^{i\Omega t'}]g_{k_m}^{\dagger}(t',0)g_k^{\dagger}(t',0). \quad \text{(B2)}$$

The vector $\vec{y}(0)$ at the initial time directly gives the density matrix at time t:

$$\tilde{g}_k^{<}(t,t) = \sum_{m=0}^{N} y_m(0)\rho y_m^{\dagger}(0). \quad \text{(B3)}$$

In order to compute the density matrix we need to evolve $\vec{y}$ backward in time with the initial condition $y_m(t) = g_k(t,0)\delta_{m0}$. The time evolution is given by a Schrödinger equation $i\partial_{t'}\vec{y}(t') = \vec{y}(t')A(t')$ with a sparse Hamiltonian matrix A:

$$A(t') = \begin{pmatrix} 0 & h_1(t') & \cdots & h_N(t') \\ h_1^{\dagger}(t') & 0 & \cdots & 0 \\ \vdots & & & \vdots \\ h_N^{\dagger}(t') & 0 & \cdots & 0 \end{pmatrix}. \quad \text{(B4)}$$

The form of the matrix allows us to compute the time evolution directly during a time interval dt when $A(t)$ may be considered constant. The integration which preserves the norm of the vector is very stable, and allows us to work with rather large time increment. Using the relation $A^3=\lambda A$ with $\lambda=\Sigma_q M_q^2/V$, one finds

$$\vec{y}(t'-dt) = \left(1 + i\frac{\sin(dt\lambda)}{\lambda}A(t') + \frac{\cos(dt\lambda)-1}{\lambda^2}A^2(t')\right)\vec{y}(t'). \quad \text{(B5)}$$

[1] J. Shah, *Ultrafast Spectroscopy of Semiconductors and Semiconductor Nanostructures* (Springer-Verlag, Berlin, 1997).
[2] L. Banyai, D. B. Tran Thoai, E. Reitsamer, H. Haug, D. Steinbach, M. U. Wehner, and M. Wegener, Phys. Rev. Lett. **75**, 2188 (1995); M. U. Wehner, M. H. Ulm, D. S. Chemla, and M. Wegener, *ibid.* **80**, 1992 (1998).
[3] C. Fürst, A. Leitenstorfer, A. Lauberau, and R. Zimmermann, Phys. Rev. Lett. **78**, 3733 (1997); A. Leitenstorder, C. Fürst, A. Laubereau, W. Kaiser, G. Tränkle, and G. Weimann, *ibid.* **76**, 1545 (1996).
[4] M. Lindberg and S. W. Koch, Phys. Rev. B **38**, 3342 (1988); H. Haug and S. W. Koch, *Quantum Theory of the Optical and Electronic Properties of Semiconductors* (World Scientific, Singapore, 1994), Chap. 12.
[5] T. Kuhn and F. Rossi, Phys. Rev. B **41**, 7496 (1992).
[6] H. Haug and A.-P. Jauho, *Quantum Kinetics in Transport and Optics of Semiconductors* (Springer-Verlag, Berlin, 1996).
[7] D. B. Tran Thoai and H. Haug, Phys. Status Solidi B **173**, 159 (1992); Phys. Rev. B **47**, 3574 (1993).
[8] L. P. Kadanoff and G. Baym, *Quantum Statistical Mechanics* (Benjamin, New York, 1962); L. V. Keldysh, Zh. Éksp. Teor. Fiz. **47**, 1515 (1964) [Sov. Phys. JETP **20**, 1018 (1965)].
[9] P. Lipavský, V. Špička, and B. Velický, Phys. Rev. B **34**, 6933 (1986).
[10] A. Schmenkel, L. Bányai, and H. Haug, J. Lumin. **76&77**, 134 (1998).
[11] Q. T. Vu, L. Bányai, H. Haug, F. X. Camescasse, J.-P. Likforman, and A. Alexandrou, Phys. Rev. B **59**, 2760 (1999).
[12] I. Balslev, R. Zimmermann, and A. Stahl, Phys. Rev. B **40**, 4095 (1989).
[13] R. Zimermann, Phys. Status Solidi B **159**, 317 (1990); R. Zimmermann and J. Wauer, J. Lumin. **58**, 271 (1994).
[14] J. Fricke, V. Meden, C. Wóhler, and K. Schönhammer, Ann. Phys. (N.Y.) **253**, 177 (1997); J. Fricke, *ibid.* **252**, 479 (1996).
[15] K. Victor, V. M. Axt, and A. Stahl, Phys. Rev. B **51**, 14 164 (1995).
[16] J. Schilp, T. Kuhn, and G. Mahler, Phys. Rev. B **50**, 5435 (1994).
[17] A. V. Kuznetsov, Phys. Rev. B **44**, 8721 (1991).
[18] C. Sieh, T. Meier, F. Jahnke, A. Knorr, S. W. Koch, P. Brick, M. Hübner, C. Ell, J. Prineas, G. Khitrova, and H. M. Gibbs, Phys. Rev. Lett. **82**, 3112 (1999).
[19] M. Hartmann and W. Schäfer, Phys. Status Solidi B **173**, 165 (1992).
[20] R. Binder, H. S. Köhler, M. Bonitz, and N. Kwong, Phys. Rev. B **55**, 5110 (1997).
[21] J. A. Kenrow and T. K. Gustafson, Phys. Rev. Lett. **77**, 3605 (1996); J. A. Kenrow, Phys. Rev. B **55**, 7809 (1997).
[22] Th. Östreich, Phys. Status Solidi **164**, 313 (1997); N. Dongalic and Th. Östreich, Phys. Rev. B **59**, 7493 (1999).
[23] P. Gartner, L. Bányai, and H. Haug, Phys. Rev. B **60**, 14 234 (1999).
[24] A. V. Kuznetsov, Ann. Phys. (N.Y.) **258**, 157 (1997).
[25] G. D. Mahan, *Many-Particle Physics* (Plenum, New York, 1990), Chap. 1.3.
[26] D. C. Langreth and J. W. Wilkins, Phys. Rev. B **6**, 3189 (1972); D. C. Langreth, in *Linear and Nonlinear Electron Transport in Solids*, edited by J. T. Devreese and V. E. van Doren (Plenum, New York, 1976).
[27] An implicit summation over repeated indices is assumed throughout the paper.
[28] V. Meden, C. Wöhler, J. Fricke, and K. Schönhammer, Phys. Rev. B **53**, 12 855 (1996).
[29] R. Zimmermann and G. Trallero-Giner, Phys. Rev. B **56**, 9488 (1997).
[30] M. Lindberg, R. Binder, and S. W. Koch, Phys. Rev. A **45**, 1865 (1992).
[31] R. Binder, S. W. Koch, M. Lindberg, W. Schäfer, and F. Jahnke, Phys. Rev. B **43**, 6520 (1991).
[32] R. Zimermann, J. Wauer, A. Leitenstorfer, and C. Fürst, J. Lumin. **76/77**, 34 (1998).
[33] I. J. Lang and Y. A. Firsov, Zh. Éksp. Teor. Fiz. **43**, 1843 (1962) [Sov. Phys. JETP **16**, 1301 (1962)].
[34] P. Hyldgaard, S. Hershfield, J. H. Davies, and J. W. Wilkins, Ann. Phys. (N.Y.) **236**, 1 (1994).
[35] H. Castella and R. Zimmermann, Phys. Rev. B **59**, R7804 (1999); T. Kuhn, V. M. Axt, M. Herbst, and E. Binder, in *Coherent Control in Atoms, Molecules, and Semiconductors* edited by W. Pötz and W. A. Schroeder (Kluwer, Dordrecht, 1999).
[36] H. Castella (unpublished).
[37] D. Steinbach, M. U. Wehner, M. Wegener, L. Bányai, E. Reitsamer, and H. Haug, Chem. Phys. **210**, 49 (1996).
[38] J.-Y. Bigot, M. T. Portella, R. W. Schoenlein, C. J. Bardeen, A. Migus, and C. V. Shank, Phys. Rev. Lett. **66**, 1138 (1991).